

# Controlling False Positives in Image Segmentation via Conformal Prediction

Luca Mossina Corentin Friedrich

IRT Saint Exupéry, Toulouse, France

## Abstract

Reliable semantic segmentation is essential for clinical decision making, yet deep models rarely provide explicit statistical guarantees on their errors. We introduce a simple post-hoc framework that constructs confidence masks with distribution-free, image-level control of false-positive predictions. Given any pretrained segmentation model, we define a nested family of shrunken masks obtained either by increasing the score threshold or by applying morphological erosion. A labeled calibration set is used to select a single shrink parameter via conformal prediction, ensuring that, for new images that are exchangeable with the calibration data, the proportion of false positives retained in the confidence mask stays below a user-specified tolerance with high probability. The method is model-agnostic, requires no retraining, and provides finite-sample guarantees regardless of the underlying predictor. Experiments on a polyp-segmentation benchmark demonstrate target-level empirical validity. Our framework enables practical, risk-aware segmentation in settings where over-segmentation can have clinical consequences. Code at <https://github.com/deel-ai-papers/conseco>.

## 1 Introduction

Reliable segmentation is a prerequisite for clinical use of deep-learning models, where false positives may trigger unnecessary interventions. Existing uncertainty scores and calibration methods provide useful heuristics, but they do not offer finite-sample guarantees on the errors of the produced masks. Given any pretrained segmentation model, our post-hoc method builds inner masks  $I_\lambda(X)$  by progressively shrinking the predicted mask  $\hat{Y}$  using a single control parameter  $\lambda$ , through either sigmoid score thresholding or morphological erosion. We calibrate the shrinkage level on a small held-out labeled set.

Our procedure, based on inductive (or “split”) Conformal Prediction (CP) [21, 15], guarantees that at a user-chosen confidence level  $1 - \alpha$ , the inner mask contains at most a user-specified fraction  $\tau$  of false-positive pixels. The validity bound is asserted at the *image level*; we refer to the inner mask  $I_\lambda(X)$  as “confidence mask” and the remainder of the prediction is flagged as uncertain, producing the uncertainty region  $U_\lambda(X) = \hat{Y} \setminus I_\lambda(X)$ .

**Contributions.** (i) A black-box, distribution-free method that returns inner prediction sets  $I_\lambda$  with guaranteed control of accepted false positives at the image level. (ii) Two concrete, implementation-ready formulations: score thresholding and morphological erosion. (iii) A calibration protocol that exposes two operational choices to the user, confidence  $1 - \alpha$

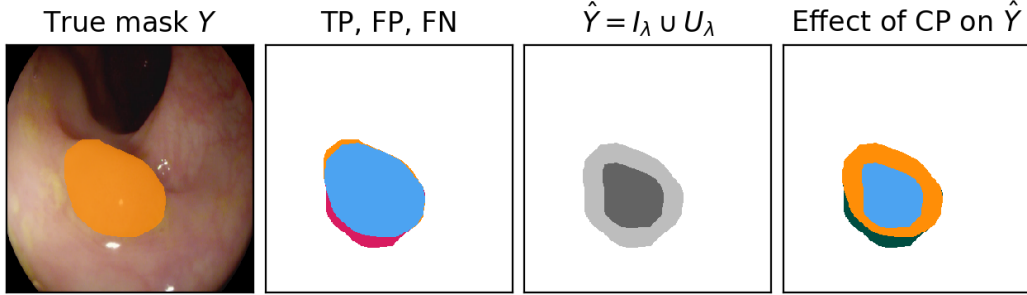


Figure 1: Example with erosion inner mask  $I_\lambda^\varepsilon(X)$  at  $\tau = 0.01$  and  $1 - \alpha = 0.9$ . From the left: (i) Ground-truth mask  $Y$  overlayed on input image  $X$ ; (ii) true positives & false positives in  $\hat{Y}$ , and  $Y$  pixels missed (false negatives); (iii) Inner “confidence” mask  $I_\lambda^\varepsilon(X)$  (dark grey) and uncertainty “rejection” mask  $U_\lambda(X)$  (light grey); (iv)  $\hat{Y}$  is shrunk to  $I_\lambda^\varepsilon(X)$ .  $U_\lambda(X)$  rejects most FPs (■) but also some TPs, i.e. g.t. pixels (■) well-segmented in  $\hat{Y}$ .

**Colors.** ■: true mask  $Y$ ; ■: false positives (FP); ■: true positives (TP); ■: rejected FPs.

and tolerated accepted false positives  $\tau$ , with no retraining. (iv) Evidence on a biomedical benchmark that the empirical image-level validity of the *accepted false-positive* proportion (AFP) matches the target confidence.

## 2 Related Work

Split CP [15] constructs distribution-free prediction sets with finite-sample guarantees of containing the true target at a user-specified confidence level  $1 - \alpha$ . Conformal Risk Control extends CP to monotone losses, providing guarantees on the expected risk [2]. In multilabel prediction, inner and outer sets are constructed to enclose the true label set [6].

For CP in semantic segmentation, [8] have used inner and outer prediction masks targeting coverage of the ground-truth mask. Other conformal approaches reduce false negatives by lowering score thresholds [2, 13, 5] or by morphological dilation of the predicted mask [14]. CP is complementary to the broader literature on uncertainty quantification: methods such as MC-Dropout [11], deep ensembles [12], or failure prediction [7] provide useful uncertainty maps but do not yield distribution-free guarantees at deployment, which can be achieved with CP.

**Our positioning.** We address binary medical segmentation and control the proportion of accepted false-positive pixels within the predicted region using nested prediction-shrunkers and conformal calibration. This is complementary to prior false-negative control work and different in scope from multilabel FP-limited set prediction [10]. We instantiate the nested sets through standard anti-extensive morphological operators [17] and sigmoid-score thresholding.

### 3 Methods

We aim to control statistically the number of false-positive pixels accepted in predicted masks. To do so, we define a quantity  $\mathcal{F}_\lambda(X, Y)$  (Eq. 3) that is compatible with the requirements of CP and hence admits rigorous statistical guarantees, notably via the inner sets proposed in Eq. 1 and Eq. 2. We refer to  $\mathcal{F}_\lambda$  as the *accepted false-positive proportion (AFP)*: it measures the fraction of false positives that remain in the accepted region relative to the original predicted area  $|\hat{Y}|$ .

Let  $X$  be an image over a grid  $\Omega \subseteq \mathbb{Z}^2$  of  $n_H \times n_W$  pixels, and let  $Y \subseteq \Omega$  and  $\hat{Y} \subseteq \Omega$  denote the ground-truth and predicted segmentation masks obtained with a segmentation model, respectively.

**Defining inner prediction sets.** We construct a nested family of *inner prediction sets*  $\{I_\lambda(X)\}_{\lambda \in \Lambda}$  such that: (i)  $I_\lambda(X) \subseteq \hat{Y}$ , (ii) there exists  $\lambda_0$  such that  $I_{\lambda_0}(X) = \hat{Y}$ , and (iii) for any  $\lambda_1 \leq \lambda_2$ ,  $I_{\lambda_1}(X) \supseteq I_{\lambda_2}(X)$ . We interpret the inner prediction sets as **confidence masks** at a chosen confidence level, defining subregions of the prediction that are “accepted” according to the conformal procedure.

We propose two simple ways to shrink a predicted mask so that fewer false-positive pixels are accepted as confident. We restrict our exposition to two inner set models that are applicable *a posteriori* to most segmentation models, although any nested family of sets (see above) can be used.

First is a set that applies a **threshold on sigmoid** scores  $\hat{\sigma}(X)_{ij}$ , the output of a binary segmentation model:

$$I_\lambda^\sigma(X) := \{\text{pixels } (i, j) \text{ s.t. } \hat{\sigma}(X)_{ij} \geq \lambda\}, \quad (1)$$

with  $\lambda \in [0.5, 1]$ , where  $\lambda_0 = 0.5$  is the threshold commonly used in segmentation.

Second, we build a set that works as a dual to the morphological dilation [17] used in [14]: we apply **morphological erosion**  $\varepsilon_B(\cdot)$  to the mask  $\hat{Y}$  as

$$I_\lambda^\varepsilon(X) := \underbrace{(\varepsilon_B \circ \varepsilon_B \circ \dots \circ \varepsilon_B)}_{\lambda \text{ iterations}}(\hat{Y}) = \varepsilon_B^\lambda(\hat{Y}). \quad (2)$$

We fix a structuring element, e.g.  $B = \begin{smallmatrix} \textcolor{blue}{\square} & \square \\ \square & \square \end{smallmatrix}$  for 4-connectivity, and erode  $\hat{Y}$   $\lambda$  times,  $\lambda \in \mathbb{N}$ ; note that for  $\lambda_0 = 0$ ,  $I_{\lambda_0}(X) = \hat{Y}$ . This erosion model also applies to black-box predictors, whose internals are not accessible to end users (e.g. third-party vendors, embedded in medical equipment, etc.). This function is suited to segmentation models where the false positives are concentrated at the boundary of the object. As noted in [14], *any* morphology-based inner set is applicable, e.g., combining structuring elements or using a discretized ball whose radius is controlled by  $\lambda$ .

**Our inner sets are nested.** Our definitions give rise to nested sets, that is, for any  $\lambda_1 \leq \lambda_2$ , we get  $I_{\lambda_1} \supseteq I_{\lambda_2}$ . For  $I_\lambda^\sigma(X)$ , as  $\lambda$  grows, fewer pixels in  $\hat{Y}$  have scores above this threshold and fewer pixels are included in  $I_\lambda^\sigma$  (Eq. 1), hence its size is non-increasing in  $\lambda$ . For  $I_\lambda^\varepsilon$ , since morphological erosion is anti-extensive (i.e. contractive), we have  $\varepsilon_B^{\lambda_1}(\hat{Y}) \supseteq \varepsilon_B^{\lambda_2}(\hat{Y})$  for  $\lambda_1 \leq \lambda_2$ .

#### 3.1 Formulation of the False-Positives Control problem

Inner sets  $I_\lambda(X)$  aim to ignore false positives in predictions. However, due to noise in predictive models or annotation errors in segmentation datasets, reaching zero false-positive pixels

would require large values of  $\lambda$ . The obtained inner sets would thus be very small or even empty; note that the trivial solution  $I_\lambda = \emptyset$  does not contain any FPs and it is always valid. To avoid this trivial solution, we allow a small fraction of FPs, which is controlled by a user-defined tolerance parameter  $\tau \in [0, 1]$ .

Let  $W(X, Y) = \hat{Y} \cap (\Omega \setminus Y)$  denote the set of **false-positive** (FP) pixels in  $\hat{Y}$ . This set does not depend on the inner mask  $I_\lambda$ . Since we cannot control the size of  $W(X, Y)$ , which depends on the fixed predictor, we instead construct inner masks that are the largest subsets of  $\hat{Y}$  containing few false positives, according to the chosen definition of inner mask (Eqs. 1–2). We refer to  $I_\lambda(X)$  as the *confidence mask* and to its complement  $U_\lambda(X) = \hat{Y} \setminus I_\lambda(X)$  as the *uncertain region*.

We want to control the following quantity, representing the **accepted false-positive proportion** (AFP) within the predicted mask  $\hat{Y}$ :

$$\mathcal{F}_\lambda(X, Y) = \frac{|I_\lambda(X) \cap W(X, Y)|}{|\hat{Y}|}. \quad (3)$$

Here  $|\cdot|$  denotes set cardinality. If  $|\hat{Y}| = 0$ , we set  $I_\lambda = \emptyset$  and  $\mathcal{F}_\lambda = 0$ . Since  $I_\lambda$  is nested and the denominator  $|\hat{Y}|$  is  $\lambda$ -invariant,  $\mathcal{F}_\lambda$  is non-increasing in  $\lambda$ . Dividing by  $|I_\lambda|$  would break this monotonicity and is therefore avoided.

**Interpretation.**  $\mathcal{F}_\lambda$  quantifies the proportion of false positives that remain “accepted” within the confidence mask at a level  $\lambda$ . For  $\lambda = \lambda_0$  (no shrinkage),  $\mathcal{F}_{\lambda_0} = |W(X, Y)|/|\hat{Y}|$  corresponds to the original false-positive fraction of the prediction. Increasing  $\lambda$  enforces stricter acceptance and can only decrease  $\mathcal{F}_\lambda$ . In practice,  $\mathcal{F}_\lambda$  expresses the fraction of spurious detections that remain unfiltered after applying the confidence threshold; in some cases it is possible to have  $\mathcal{F}_\lambda(X, Y) \leq \tau$ , in which case no shrinkage would be needed.

### 3.2 Conformal Prediction

Our method builds on the standard inductive CP framework [15]. We adapt the inner sets from the segmentation approach of [8], and use morphological erosion as the counterpart of the dilation-based outer sets in [14]. Importantly, CP provides *marginal frequentist* guarantees on the *mask-level procedure*, rather than on individual pixels: if the calibration and testing process were repeated many times, the empirical validity condition in Eq. (6) would be satisfied in at least  $100(1 - \alpha)\%$  of cases on average. This states that, for exchangeable data, the accepted false-positive proportion (AFP) of the inner mask satisfies  $\mathcal{F}_{\hat{\lambda}} \leq \tau$  with probability at least  $1 - \alpha$  at the image level. Once the user has fixed a tolerance value  $\tau \in [0, 1]$ , the nonconformity score  $r_\iota = r(X_\iota, Y_\iota)$  for a calibration pair  $(X_\iota, Y_\iota)$  is computed as (details in Sec. 3.3)

$$r_\iota = \inf \{ \lambda : \mathcal{F}_\lambda(X_\iota, Y_\iota) \leq \tau \}, \quad (4)$$

and the conformalizing quantile is the

$$\hat{\lambda} = \lceil (n + 1)(1 - \alpha) \rceil \text{-th smallest value in } (r_\iota)_{\iota=1}^n. \quad (5)$$

Assuming that calibration data and test point  $(X_{\text{new}}, Y_{\text{new}})$  form an exchangeable (or i.i.d.) sequence, we obtain the distribution-free, marginal guarantee:

$$\mathbb{P}(\mathcal{F}_{\hat{\lambda}}(X_{\text{new}}, Y_{\text{new}}) \leq \tau) \geq 1 - \alpha. \quad (6)$$

**Proof.** Because inner masks  $I_\lambda(X)$  are nested with respect to  $\lambda$ ,  $\mathcal{F}_\lambda$  is non-increasing in  $\lambda$ . Define the binary loss  $\ell(X, Y, \lambda) = \mathbb{1}\{\mathcal{F}_\lambda(X, Y) > \tau\}$ , which is monotone non-increasing in  $\lambda$ . Applying Conformalized Risk Control [2] with this loss, whose CRC selection rule coincides with the conformal quantile (Sec. 2.3 in [2]), yields Eq. (6).

**Interpretation.** This image-level guarantee states that, with probability (i.e. confidence level) at least  $1 - \alpha$ , the region of the inner mask  $I_{\hat{\lambda}}(X_{\text{new}})$  will not “accept” more than a fraction  $\tau$  (e.g., 5%) false positives in the original prediction  $\hat{Y}_{\text{new}}$ . This can also be seen as a mechanism to produce confidence regions that mitigate the operational hazard of predicting a treatment (i.e. a “positive” pixel) where not needed. Clinically, AFP bounds the fraction of unnecessary positive pixels *within the region we agree to act upon*, while the rejected pixels are marked as uncertain and not acted on.

**Scope.** Our guarantee depends only on exchangeability of the data and on the nestedness of the inner sets  $I_\lambda(X)_{\lambda \in \Lambda}$ . It does not depend on the particular way  $I_\lambda$  is produced. Any scoring function or post-hoc shrinker that induces a nested family can be plugged in; this choice affects only *utility* (e.g., average contraction, inner-margin size, ATP/CR), not validity. The convention of a fixed denominator  $|\hat{Y}|$  and the handling of empty masks ( $\mathcal{F}_\lambda = 0$ ) likewise do not change the guarantee; they only influence how conservative the resulting inner masks are. This opens the method to empirical exploration of shrinkers and scores from any uncertainty model.

### 3.3 Conformalization procedure

One can use any fixed segmentation model, either pretrained or trained separately on dedicated data.

1. **Collect calibration data.** Gather a labeled calibration set  $\{(X_\iota, Y_\iota)\}_{\iota=1}^n$ , distinct from both training and test data. Following standard CP assumptions, these samples are required to be exchangeable (or i.i.d.) with the test cases.
2. **Define the family of inner sets.** Select either: (i) the threshold model  $I_\lambda^\sigma$  in Eq. (1) with  $\Lambda = [0.5, 1]$  or (ii) the morphological model  $I_\lambda^\varepsilon$  in Eq. (2) with  $\Lambda = \mathbb{N}$  and a structuring element, e.g.  $B = \begin{smallmatrix} \square & \square \\ \square & \square \end{smallmatrix}$  or  $\begin{smallmatrix} \square & \square \\ \square & \square \end{smallmatrix}$ .
3. **Compute calibration scores.** For each calibration pair  $(X_\iota, Y_\iota)$ , compute  $r_\iota = r(X_\iota, Y_\iota)$  as in Eq. (4).
  - (i) For  $I_\lambda^\sigma$ , evaluate  $\mathcal{F}_\lambda$  at breakpoints  $\lambda \in \{\hat{\sigma}(X_\iota)_{ij} : (i, j) \in \hat{Y}_\iota\} \cup \{1\}$  and keep the smallest  $\lambda$  s.t.  $\mathcal{F}_\lambda \leq \tau$ .
  - (ii) For  $I_\lambda^\varepsilon$ , iterate  $\varepsilon_B$  until  $\mathcal{F}_\lambda \leq \tau$  or the mask becomes empty, in which case  $\mathcal{F}_\lambda = 0$ .
4. **Estimate the conformal threshold.** Let  $k = \lceil (n+1)(1-\alpha) \rceil$ , and set  $\hat{\lambda}$  to the  $k$ -th smallest value among the calibration scores  $\{r_\iota\}_{\iota=1}^n$ , as in Eq. (5).
5. **Predict on the test set.** For a new input  $X_{\text{new}}$ , output the inner mask  $I_{\hat{\lambda}}(X_{\text{new}})$ .

## 4 Experiments

Following prior work on distribution-free methods for segmentation [3, 2, 5], we evaluate on the POLYPS dataset collection [18, 4, 19, 20, 16] using pretrained PraNet [9].<sup>1</sup> We compare three procedures: *Baseline* (uncalibrated sigmoid threshold at 0.5, i.e.,  $I_{\lambda_0} = \hat{Y}$ ), *Threshold* (CP by increasing the score cutoff), and *Erosion* (CP by morphological erosion). Confidence level is  $1 - \alpha = 0.90$  and tolerance  $\tau \in \{0.1, 0.01, 0.001\}$ . For erosion we use a cross structuring element  $B = \begin{smallmatrix} \textcolor{blue}{\square} & \square \\ \square & \textcolor{blue}{\square} \end{smallmatrix}$ . Each run randomly permutes the test split and assigns half to calibration and half to evaluation, yielding 250 calibration images. We report mean  $\pm$  standard deviation over 10 seeds.

**Metrics.** We quantify validity and utility with three image-level quantities. (i) *Empirical validity* (EV): fraction of test images whose accepted false-positive proportion does not exceed  $\tau$ , that targets the nominal frequency  $1 - \alpha$ ,

$$\text{EV} = \frac{1}{n_{\text{test}}} \sum_{i=1}^{n_{\text{test}}} \mathbb{1}\{\mathcal{F}_{\hat{\lambda}}(X_i, Y_i) \leq \tau\}. \quad (7)$$

(ii) *Contraction ratio* (CR): retained area after shrinkage,

$$\text{CR} = \frac{1}{n_{\text{test}}} \sum_{i=1}^{n_{\text{test}}} \frac{|I_{\hat{\lambda}}(X_i)|}{|\hat{Y}_i|}. \quad (8)$$

CR = 1 for the Baseline and decreases as masks shrink, measuring the utility loss incurred by enforcing statistical validity.

(iii) *Accepted true-positive fraction* (ATP):

$$\text{ATP} = \frac{1}{n_{\text{test}}} \sum_{i=1}^{n_{\text{test}}} \frac{|I_{\hat{\lambda}}(X_i) \cap Y_i|}{|\hat{Y}_i|}. \quad (9)$$

For the Baseline,  $\text{ATP} = \frac{|TP|}{|\hat{Y}|}$  equals image-level precision, i.e. the fraction of TPs in the prediction mask.

### 4.1 Results

Quantitative results at  $1 - \alpha = 0.9$  are reported in Tab. 1. Conformalized procedures attain empirical validity (EV) close to the nominal target across all  $\tau$ , whereas the Baseline fails for small  $\tau$  and only approaches validity in the more permissive setting  $\tau = 0.1$ , confirming the need for calibration. Utility decreases smoothly as  $\tau$  tightens. At fixed  $\tau$ , the Threshold variant retains higher CR and ATP than Erosion, reflecting a more moderate shrinkage path on typical polyp masks, while Erosion removes a larger fraction of peripheral predictions. This is expected, as sigmoid scores are often more informative than the binary mask; when available, they should be evaluated alongside erosion. The validity-utility trade-off behaves monotonically and remains stable across random seeds. Finally, since Conformal Prediction guarantees statistical validity for *any* segmentation model, utility metrics can also serve to compare or select among different predictors, e.g. when provided by a third-party.

<sup>1</sup>We use the precomputed predictions as distributed by the authors of [3, 2] for their comprehensive introduction to CP [1] at [github.com/aangelopoulos/conformal-prediction](https://github.com/aangelopoulos/conformal-prediction),

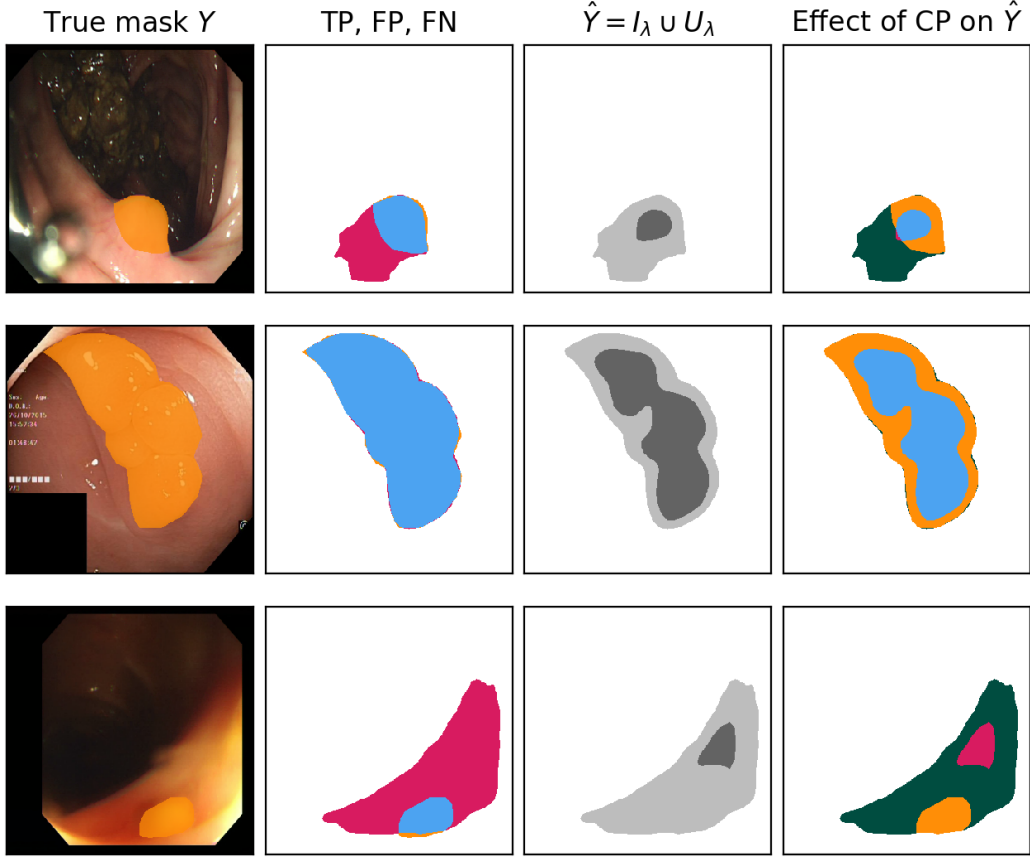


Figure 2: Examples with thresholding inner mask  $I_\lambda^\sigma(X)$ , at  $\tau = 0.01$  and  $1 - \alpha = 0.9$ . **Top.** Large FP removal with moderate TP loss. **Middle.** When FPs are already negligible, shrinkage removes TPs. **Bottom.** Failure case: residual inner mask is FP-only.  
**Colors.** ■: true mask  $Y$ ; ■: false positives; ■: true positives; ■: rejected false positives.

## 5 Conclusion and Perspectives

We introduced a post-hoc conformal procedure for binary segmentation that calibrates a single shrink parameter to control, with finite-sample guarantees, the image-level proportion of accepted false positives. The method is model-agnostic, requires no retraining, and operates with either score-thresholding or morphological-erosion shrinkers. Experiments on polyp segmentation demonstrate target-level empirical validity and a smooth validity–utility trade-off governed by  $\tau$ . Limitations include the mask-level (marginal) nature of the guarantees and potential true-positive loss when predictions are already precise. Future work includes extending the approach to multi-class segmentation and building size- and instance-adaptive inner masks.

	Method	EV	CR ( $\uparrow$ )	ATP ( $\uparrow$ )
$\tau = 0.1$	Baseline	$0.789 \pm 0.015$	—	$0.873 \pm 0.014$
	Threshold	$0.931 \pm 0.049$	$0.701 \pm 0.129$	$0.676 \pm 0.111$
	Erosion	$0.897 \pm 0.030$	$0.578 \pm 0.155$	$0.527 \pm 0.132$
$\tau = 0.01$	Baseline	$0.165 \pm 0.013$	—	$0.873 \pm 0.014$
	Threshold	$0.926 \pm 0.037$	$0.532 \pm 0.087$	$0.525 \pm 0.083$
	Erosion	$0.902 \pm 0.034$	$0.274 \pm 0.085$	$0.252 \pm 0.075$
$\tau = 0.001$	Baseline	$0.005 \pm 0.002$	—	$0.873 \pm 0.014$
	Threshold	$0.914 \pm 0.029$	$0.473 \pm 0.067$	$0.469 \pm 0.065$
	Erosion	$0.911 \pm 0.033$	$0.112 \pm 0.052$	$0.103 \pm 0.045$

Table 1: Results for confidence level  $1 - \alpha = 0.9$ .

## Acknowledgments

This work was carried out within the DEEL project,<sup>2</sup> which is part of IRT Saint Exupéry and the ANITI AI cluster. The authors acknowledge the financial support from DEEL’s Industrial and Academic Members and the France 2030 program – Grant agreements n°ANR-10-AIRT-01 and n°ANR-23-IACL-0002.

## References

- [1] ANGELOPOULOS, A. N., AND BATES, S. A gentle introduction to conformal prediction and distribution-free uncertainty quantification. *arXiv preprint arXiv:2107.07511* (2021).
- [2] ANGELOPOULOS, A. N., BATES, S., FISCH, A., LEI, L., AND SCHUSTER, T. Conformal risk control. In *The Twelfth International Conference on Learning Representations* (2024).
- [3] BATES, S., ANGELOPOULOS, A., LEI, L., MALIK, J., AND JORDAN, M. Distribution-free, risk-controlling prediction sets. *J. ACM* 68, 6 (9 2021).
- [4] BERNAL, J., SÁNCHEZ, F. J., FERNÁNDEZ-ESPARRACH, G., GIL, D., RODRÍGUEZ, C., AND VILARIÑO, F. Wm-dova maps for accurate polyp highlighting in colonoscopy: Validation vs. saliency maps from physicians. *Comp. Med. Imaging Graph.* 43 (2015), 99–111.
- [5] BLOT, V., ANGELOPOULOS, A. N., JORDAN, M., AND BRUNEL, N. J.-B. Automatically adaptive conformal risk control. In *Proceedings of The 28th International Conference on Artificial Intelligence and Statistics* (May 2025), vol. 258 of *PMLR*, pp. 19–27.
- [6] CAUCHOIS, M., GUPTA, S., AND DUCHI, J. C. Knowing what you know: valid and validated confidence sets in multiclass and multilabel prediction. *Journal of Machine Learning Research* 22, 81 (2021), 1–42.

<sup>2</sup><https://www.deel.ai>

- [7] CORBIÈRE, C., THOME, N., BAR-HEN, A., CORD, M., AND PÉREZ, P. Addressing failure prediction by learning model confidence. In *Advances in Neural Information Processing Systems* (2019), vol. 32, Curran Associates, Inc.
- [8] DAVENPORT, S. Conformal confidence sets for biomedical image segmentation. *arXiv preprint arXiv:2410.03406* (2024).
- [9] FAN, D.-P., JI, G.-P., ZHOU, T., CHEN, G., FU, H., SHEN, J., AND SHAO, L. Pranet: Parallel reverse attention network for polyp segmentation. In *MICCAI 2020* (2020), Springer, pp. 263–273.
- [10] FISCH, A., SCHUSTER, T., JAAKKOLA, T., AND BARZILAY, D. Conformal prediction sets with limited false positives. In *Proceedings of the 39th International Conference on Machine Learning* (17–23 Jul 2022), vol. 162 of *Proceedings of Machine Learning Research*, PMLR, pp. 6514–6532.
- [11] GAL, Y., AND GHAHRAMANI, Z. Dropout as a bayesian approximation: Representing model uncertainty in deep learning. In *Proceedings of The 33rd International Conference on Machine Learning* (New York, New York, USA, 20–22 Jun 2016), vol. 48 of *Proceedings of Machine Learning Research*, PMLR, pp. 1050–1059.
- [12] LAKSHMINARAYANAN, B., PRITZEL, A., AND BLUNDELL, C. Simple and scalable predictive uncertainty estimation using deep ensembles. *Advances in neural information processing systems 30* (2017).
- [13] MOSSINA, L., DALMAU, J., AND ANDÉOL, L. Conformal semantic image segmentation: Post-hoc quantification of predictive uncertainty. In *Proceedings of the IEEE/CVF Conference on Computer Vision and Pattern Recognition (CVPR) Workshops* (June 2024), pp. 3574–3584.
- [14] MOSSINA, L., AND FRIEDRICH, C. Conformal prediction for image segmentation using morphological prediction sets. In *Medical Image Computing and Computer Assisted Intervention – MICCAI 2025* (Cham, 2026), Springer Nature Switzerland, pp. 78–88.
- [15] PAPADOPOULOS, H., PROEDROU, K., VOVK, V., AND GAMMERMAN, A. Inductive confidence machines for regression. In *ECML 2002* (2002).
- [16] POGORELOV, K., RANDEL, K. R., GRIWODZ, C., ESKELAND, S. L., DE LANGE, T., ET AL. Kvasir: A multi-class image dataset for computer aided gastrointestinal disease detection. In *Proceedings of ACM MMSys* (2017), p. 164–169.
- [17] SERRA, J. *Image analysis and mathematical morphology: V.1*. Academic Press, 1984.
- [18] SILVA, J., HISTACE, A., ROMAIN, O., DRAY, X., AND GRANADO, B. Toward embedded detection of polyps in wce images for early diagnosis of colorectal cancer. *Int J CARS 9* (2014), 283–293.
- [19] TAJBAKHSH, N., GURUDU, S. R., AND LIANG, J. Automated polyp detection in colonoscopy videos using shape and context information. *IEEE T-MI 35*, 2 (2015), 630–644.

- [20] VÁZQUEZ, D., BERNAL, J., SÁNCHEZ, F. J., FERNÁNDEZ-ESPARRACH, G., LÓPEZ, A. M., ROMERO, A., ET AL. A benchmark for endoluminal scene segmentation of colonoscopy images. *J Healthc Eng* 2017, 1 (2017), 4037190.
- [21] VOVK, V., GAMMERMAN, A., AND SHAFER, G. *Algorithmic learning in a random world*, vol. 29. Springer, 2005.